Journal of Solid State Chemistry 182 (2009) 2046–2052

Contents lists available at ScienceDirect

Journal of Solid State Chemistry

journal homepage: www.elsevier.com/locate/jssc

Synthesis and structure analysis of tetragonal $Li_7La_3Zr_2O_{12}$ with the garnet-related type structure

Junji Awaka *[,1], Norihito Kijima, Hiroshi Hayakawa, Junji Akimoto

National Institute of Advanced Industrial Science and Technology (AIST), Tsukuba Central 5, 1-1-1 Higashi, Tsukuba, Ibaraki 305-8565, Japan

ARTICLE INFO

Article history:
Received 17 February 2009
Received in revised form
27 April 2009
Accepted 17 May 2009
Available online 22 May 2009

Keywords:
Garnet
Crystal growth
Single-crystal X-ray diffraction
Neutron powder diffraction
X-ray powder diffraction
Lithium-ion conductor

ABSTRACT

We have successfully synthesized a high-purity polycrystalline sample of tetragonal $Li_7La_3Zr_2O_{12}$. Single crystals have been also grown by a flux method. The single-crystal X-ray diffraction analysis verifies that tetragonal $Li_7La_3Zr_2O_{12}$ has the garnet-related type structure with a space group of $I4_1/acd$ (no. 142). The lattice constants are $a = 13.134(4)$ Å and $c = 12.663(8)$ Å. The garnet-type framework structure is composed of two types of dodecahedral LaO_8 and octahedral ZrO_6. Li atoms occupy three crystallographic sites in the interstices of this framework structure, where Li(1), Li(2), and Li(3) atoms are located at the tetrahedral 8*a* site and the distorted octahedral 16*f* and 32*g* sites, respectively. The structure is also investigated by the Rietveld method with X-ray and neutron powder diffraction data. These diffraction patterns are identified as the tetragonal $Li_7La_3Zr_2O_{12}$ structure determined from the single-crystal data. The present tetragonal $Li_7La_3Zr_2O_{12}$ sample exhibits a bulk Li-ion conductivity of $\sigma_b = 1.63 \times 10^{-6}$ S cm^{-1} and grain-boundary Li-ion conductivity of $\sigma_{gb} = 5.59 \times 10^{-7}$ S cm^{-1} at 300 K. The activation energy is estimated to be $E_a = 0.54$ eV in the temperature range of 300–560 K.

© 2009 Elsevier Inc. All rights reserved.

1. Introduction

Over the last decade, rechargeable lithium-ion batteries have become a crucial component of a number of portable electronic devices as well as large electrical power storage systems. Notable examples include mobile phones, notebook computers, and hybrid vehicles. Recent interest in all-solid-state rechargeable Li-ion batteries has spurred a great deal of research into solid-state Li-ion conductors with various crystal structures. Recently, $Li_7La_3Zr_2O_{12}$ having a garnet-related type structure was reported as a fast Li-ion conductor with high bulk conductivity σ_b around 10^{-4} S cm^{-1} at 298 K [1]. This electrolyte is a good candidate for all-solid-state rechargeable Li-ion batteries, particularly because of its good thermal performance and chemical stability. The compound was synthesized at 1503 K, and the structure was reported to have cubic symmetry with a lattice constant of $a = 12.9682(6)$ Å.

In the present study, we succeeded in synthesizing $Li_7La_3Zr_2O_{12}$ with a tetragonal symmetry for the first time by heating at a relatively low temperature of 1253 K. It is widely recognized that garnet-related lithium-ion conducting oxides show cubic symmetry of *Ia*–3*d* (no. 230) [1–8], and no garnet-related lithium-ion conducting oxides with tetragonal symmetry have been reported to date. We also successfully grew single crystals of tetragonal $Li_7La_3Zr_2O_{12}$ by a flux method, and determined the crystal structure by single-crystal X-ray structure analysis. We confirmed the determined crystal structure by the Rietveld method using X-ray and neutron powder diffraction data.

2. Experimental

Polycrystalline tetragonal $Li_7La_3Zr_2O_{12}$ was prepared by the solid-state reaction:

$$7Li_2CO_3 + 3La_2O_3 + 4ZrO_2 \rightarrow 2Li_7La_3Zr_2O_{12} + 7CO_2 \uparrow . \quad (1)$$

The starting materials (purity: 99.9%) of Li_2CO_3, La_2O_3 (pre-dried at 1173 K for 12 h), and ZrO_2 were mixed in the calculated ratio, where 10 wt% excess Li_2CO_3 was added to prevent the loss of the lithium component by volatilization at high temperature. Mixed powder materials were put in an alumina crucible and heated at 1173 K for 5 h in ambient atmosphere. The calcined specimen was reground and heated at 1253 K for 5 h.

Single-crystal growth was conducted by a flux method. The starting materials were as-prepared $Li_7La_3Zr_2O_{12}$ and Li_2CO_3 as a flux. These materials were well-mixed in the nominal weight ratio of $Li_7La_3Zr_2O_{12}$:$Li_2CO_3 = 1$:1. The powder mixture was charged into a gold crucible, and the temperature was elevated to 1313 K at the rate of 200 K h^{-1}, and then held for 48 h. The crystals were separated from the solidified melts by immersing the gold crucible in hot water.

* Corresponding author.
E-mail address: j.awaka@aist.go.jp (J. Awaka).
[1] Research Fellow of the Japan Society for the Promotion of Science.

0022-4596/$ - see front matter © 2009 Elsevier Inc. All rights reserved.
doi:10.1016/j.jssc.2009.05.020

Chemical analysis of the Li, La, and Zr content of the products was carried out using inductively coupled plasma-optical emission spectroscopy (ICP-OES) using an Optima 3000 (Perkin Elmer). The morphology and chemical composition of single crystals were investigated using scanning electron microscopy-energy dispersive X-ray analysis (SEM-EDX) with a JSM-5400 scanning electron microscope equipped with a JED-2100 energy-dispersive spectrometer (JEOL).

The structure was carefully investigated by single-crystal X-ray diffraction. The intensity data were collected in 2θ–ω scan mode at a scan rate of $2.0^\circ\,\mathrm{min}^{-1}$ at 293 K on a four-circle diffractometer (Rigaku AFC-7S, operating conditions: 50 kV, 30 mA) using graphite-monochromatized Mo$K\alpha$ radiation ($\lambda = 0.71073$ Å). All calculations were carried out using a computer program XTAL3.7.2 [9].

X-ray powder diffraction (XRD) data were collected at room temperature using a Rigaku RINT2550 V diffractometer equipped with a curved graphite monochromator. The open angle of the divergence and scattering slits were both 0.5°, and the width of the receiving slit was 0.15 mm. The X-ray (Cu$K\alpha$ radiation) tube voltage and tube electric current were 40 kV and 100 mA, respectively. Diffraction data were collected at step intervals of 0.02° over a 2θ range from 5° to 120°. The fixed counting time in the XRD measurements was 2 s.

The neutron powder diffraction (ND) data were collected at room temperature using a Kinken powder diffractometer for high efficiency and high resolution measurements, HERMES, at the Institute for Materials Research (IMR), Tohoku University, installed at the JRR-3M reactor of the Japan Atomic Energy Agency (JAEA), Tokai [10]. Neutrons with a wavelength of 1.8204(5) Å were obtained by the 3 3 1 reflection of the Ge monochromator. Diffraction data were collected at step intervals of 0.1° over a 2θ range from 7° to 157°.

The XRD and ND data were analyzed by the Rietveld method with a computer program RIETAN-2000 [11]. The split pseudo-Voigt profile function was used as the profile function in the refinement. A partial profile relaxation with a modified split pseudo-Voigt function was applied to some reflections [11]. The distribution of nuclear scattering length density was calculated by the maximum entropy method (MEM) based on the Rietveld analysis using ND data. The MEM calculation was carried out with the unit cell divided into $128 \times 128 \times 128$ pixels using a MEM-analysis program PRIMA [12]. The crystal structure and MEM images were drawn using a computer program VESTA [13].

AC impedance measurements were conducted using a Solartron 1260 impedance analyzer operating at 100 mV applied AC amplitude, at 13 MHz to 100 mHz frequencies, over the temperature range of 300–560 K in air. The powder sample was pressed into a pellet at 0.2 GPa at room temperature. The pellet was covered with a powder of the same composition, and then sintered at 1273 K for 4 h. The sintered pellet was ground to a thin pellet using a diamond file. The obtained pellet was 12.11 mm in diameter and 0.97 mm thick, and the relative density of the sintered sample was 60%. The electrode connections were 8 mm in diameter, and were made from Au paste heated at 923 K for 10 min.

3. Results and discussion

3.1. Chemical analysis

The fine-powder specimen of tetragonal $Li_7La_3Zr_2O_{12}$ was white in color. Its chemical composition was determined to be Li:La:Zr = 7.0:3.0:1.9 in atomic ratio by ICP-OES, and the analytically verified chemical composition was $Li_7La_3Zr_2O_{12}$. The estimated value of oxygen content from the experimental value of Li (5.7 wt%), La (49 wt%), and Zr (20 wt%) was in good agreement with the calculated value for $Li_7La_3Zr_2O_{12}$ within the experimental error. From the compensation of electric charge, oxygen content was also calculated to be about 12 for Li:La:Zr = 7.0:3.0:1.9.

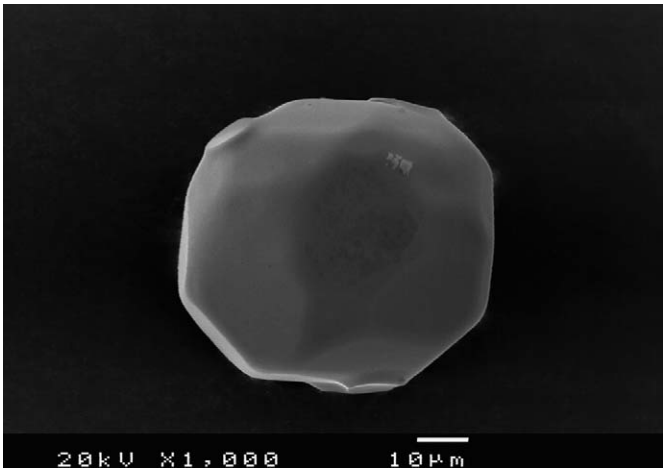

Fig. 1. SEM micrograph of a single-crystal tetragonal $Li_7La_3Zr_2O_{12}$. The scale bar is 10 μm long.

Fig. 1 shows a typical SEM micrograph of a single crystal of tetragonal $Li_7La_3Zr_2O_{12}$. The grown single crystal was transparent, had a nearly spherical shape, and had a maximum diameter of about 50 μm. EDX analysis indicated that the single crystals were free from aluminum or gold contamination from the alumina and gold crucibles. The atomic ratio of La:Zr in the single crystals was 3.0:2.0.

3.2. Single crystal X-ray diffraction analysis

The single-crystal X-ray diffraction data from tetragonal $Li_7La_3Zr_2O_{12}$ indicated an extinction rule assigned to $I4_1/acd$ (no. 142). This space group is a maximal subgroup of Ia–$3d$, and thus would allow the garnet-type structure to be maintained. No intensity which would require symmetry reduction, such as $I4_1/a$ (no. 88) shown in the majorite-type garnets [14,15], was observed.

The crystal structure of tetragonal $Li_7La_3Zr_2O_{12}$ was carefully investigated by single-crystal X-ray diffraction analysis using the computer program XTAL3.7.2. In the first stage of structural refinement, we attempted to make an accurate description of the Li-excluded framework structure. Here, the garnet-type structure was adapted as an initial structure model. In ideal garnets (space group: Ia–$3d$), the general structural formula can be represented as $\{C_3\}[A_2](D_3)O_{12}$, where C (24c), A (16a), and D (24d) sites are the cation sites, which are surrounded by oxygen atoms in a dodecahedral, octahedral, and tetrahedral arrangement, respectively [16–19]. For the present tetragonal $Li_7La_3Zr_2O_{12}$, the initial structure model was refined to the garnet-type framework structure composed of dodecahedral $La(1)O_8$, $La(2)O_8$, and octahedral ZrO_6. Other arrangements of the two kinds of cations were impossible, because the R-values and the structural parameters did not improve. The R-values reached $R = 0.049$ and $wR = 0.048$ in the first stage.

Subsequently, the differential-Fourier map was determined in order to reveal the Li sites. The decided framework structure accommodates Li atoms using a combination of two tetrahedral, two octahedral, and a trigonal prismatic coordination, where the octahedral and trigonal prismatic sites are the vacant sites of ideal

Table 1
Experimental and crystallographic data from single-crystal tetragonal $Li_7La_3Zr_2O_{12}$ at 293 K.

Chemical formula	$Li_7La_3Zr_2O_{12}$
Crystal system	Tetragonal
Space group	$I4_1/acd$ (no. 142)
Z	8
Lattice constant a (Å)	13.134(4)
Lattice constant c (Å)	12.663(8)
Cell ratio c/a	0.9641
V (Å^3)	2185(2)
D_x (g cm^{-3})	5.106
Formula weight	839.7
Max 2θ (deg)	90
Absorption correction	Spherical crystal
Transmission factors	Max: 0.622, min: 0.611
Number of variables	59
Independent reflections	2260 ($R_{int} = 0.065$)
Observed reflections ($>4\sigma$)	1311
R	0.042
wR [w $= 1/\sigma^2 F$]	0.032

Table 2
Structure parameters determined from single-crystal data for tetragonal $Li_7La_3Zr_2O_{12}$.

Atom	Site	g	x	y	z	U_{eq} (Å^2)
La(1)	8*b*	1	0	1/4	1/8	0.0059(2)
La(2)	16*e*	1	0.12716(5)	0	1/4	0.0057(2)
Zr	16*c*	1	0	0	0	0.0050(3)
Li(1)	8*a*	1	0	1/4	3/8	0.05(2)
Li(2)	16*f*	1	0.1813(13)	0.4313(13)	1/8	0.035(10)
Li(3)	32*g*	1	0.0796(12)	0.0863(11)	0.8099(12)	0.021(8)
O(1)	32*g*	1	−0.0335(3)	0.0546(3)	0.1528(3)	0.007(2)
O(2)	32*g*	1	0.0534(3)	0.8525(3)	0.5366(4)	0.008(2)
O(3)	32*g*	1	0.1499(3)	0.0273(3)	0.4454(3)	0.007(2)

garnet. In the present tetragonal $Li_7\{La_3\}[Zr_2]O_{12}$, additional Li sites were observed at the tetrahedral 8*a* site and the octahedral 16*f* and 32*g* sites as significant positive residual peaks. No significant peak was detected for the other tetrahedron or the trigonal prism.

Finally, the 8*a*, 16*f*, and 32*g* Li sites were introduced to the framework structure model, and another structure analysis was performed. Table 1 summarizes the final *R*-values and other experimental and crystallographic data. The final *R*-values, $R = 0.042$ and w$R = 0.032$, decreased from those of the Li-excluded model. Table 2 lists the final structure parameters determined from the single-crystal data. The chemical composition estimated from the present structure refinement was consistent with $Li_7La_3Zr_2O_{12}$. Li atoms showed large atomic displacement parameters. Table 3 presents anisotropic atomic displacement parameters. The thermal ellipsoids for each Li atom expanded along the elongation direction of the coordination polyhedron. Adapting the split-atom model for Li sites did not improve the *R*-values or the structural parameters. In cubic garnet-related oxides with high Li-ion conductivity, Li atoms similarly indicated large atomic displacement parameters [2–5].

Fig. 2 shows the crystal structure of tetragonal $Li_7La_3Zr_2O_{12}$. The lattice constants were $a = 13.134(4)$ Å and $c = 12.663(8)$ Å with a cell ratio of $c/a = 0.9641$, as presented in Table 1. This structure was only slightly distorted from the cubic garnet-type framework structure, leaving the garnet-type framework structure unchanged. The garnet-type framework structure was composed of dodecahedral La(1)O_8, La(2)O_8, and octahedral ZrO_6. Table 4 presents the selected interatomic distances calculated

Table 3
Anisotropic atomic displacement parameters determined from single-crystal data for tetragonal $Li_7La_3Zr_2O_{12}$.

Atom	U_{11} (Å^2)	U_{22} (Å^2)	U_{33} (Å^2)	U_{12} (Å^2)	U_{13} (Å^2)	U_{23} (Å^2)
La(1)	0.00535(14)	U_{11}	0.0070(2)	0.0003(2)	0	0
La(2)	0.0047(2)	0.0057(2)	0.0067(2)	0	0	0.0009(2)
Zr	0.0042(3)	0.0041(3)	0.0067(3)	0.0003(2)	−0.0003(3)	−0.0002(3)
Li(1)	0.027(11)	U_{11}	0.08(3)	0	0	0
Li(2)	0.031(8)	U_{11}	0.042(14)	−0.001(11)	0.012(10)	$-U_{13}$
Li(3)	0.018(8)	0.030(9)	0.016(7)	−0.008(6)	−0.010(6)	0.005(7)
O(1)	0.005(2)	0.009(2)	0.006(2)	0.0014(14)	−0.0013(14)	−0.001(2)
O(2)	0.011(2)	0.004(2)	0.010(2)	−0.0004(14)	−0.001(2)	0.000(2)
O(3)	0.007(2)	0.005(2)	0.008(2)	0.0001(13)	−0.001(2)	0.002(2)

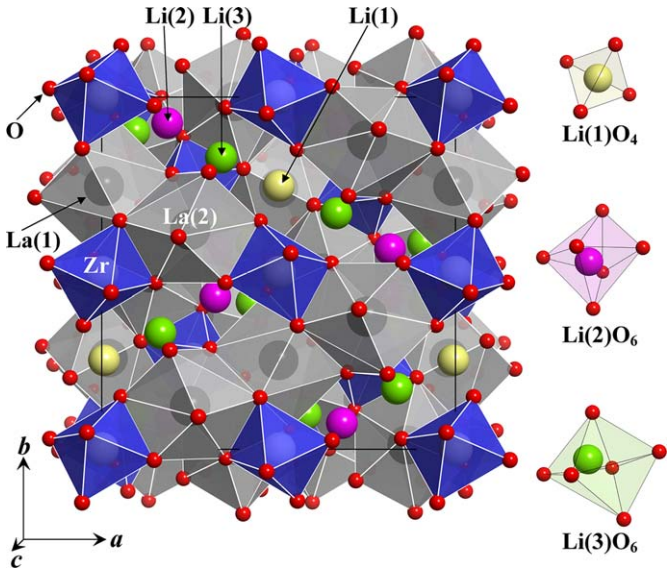

Fig. 2. Crystal structure of tetragonal $Li_7La_3Zr_2O_{12}$. The solid box indicates the unit cell.

Table 4
Selected interatomic distances (Å) calculated from single-crystal data for tetragonal $Li_7La_3Zr_2O_{12}$.

La(1)O_8	La(1)–O(1)	× 4	2.628(4)
	La(1)–O(2)$^{(a)}$	× 4	2.548(4)
La(2)O_8	La(2)–O(1)	× 2	2.546(4)
	La(2)–O(2)$^{(b)}$	× 2	2.643(4)
	La(2)–O(3)$^{(c)}$	× 2	2.469(4)
	La(2)–O(3)	× 2	2.518(4)
ZrO_6	Zr–O(1)	× 2	2.110(4)
	Zr–O(2)$^{(a)}$	× 2	2.112(4)
	Zr–O(3)$^{(d)}$	× 2	2.117(4)
Li(1)O_4	Li(1)–O(2)$^{(e)}$	× 4	1.886(4)
Li(2)O_6	Li(2)–O(1)$^{(f)}$	× 2	1.98(2)
	Li(2)–O(3)$^{(g)}$	× 2	2.375(6)
	Li(2)–O(3)$^{(h)}$	× 2	2.45(2)
Li(3)O_6	Li(3)–O(1)$^{(i)}$	× 1	2.00(2)
	Li(3)–O(1)$^{(j)}$	× 1	2.12(2)
	Li(3)–O(2)$^{(k)}$	× 1	2.13(2)
	Li(3)–O(2)$^{(l)}$	× 1	2.81(2)
	Li(3)–O(2)$^{(m)}$	× 1	2.88(2)
	Li(3)–O(3)$^{(n)}$	× 1	1.89(2)

Symmetry codes. (a) $x, 1-y, 1/2-z$; (b) $-3/4+y, -1/4+x, 3/4-z$; (c) $1/4+y, 1/4-x, -1/4+z$; (d) $x, -y, 1/2-z$; (e) $-x, 1-y, 1-z$; (f) $-x, 1/2-y, z$; (g) $1/4-y, 1/4+x, 3/4-z$; (h) $1/4-y, 3/4-x, -1/4+z$; (i) $-x, -y, 1-z$; (j) $-x, y, 1/2+z$; (k) $x, 1-y, 3/2-z$; (l) $3/4-y, 1/4-x, 1/4+z$; (m) $-3/4+y, 1/4+x, 1/4+z$; (n) $1/4-y, 1/4-x, 5/4-z$.

from the single-crystal data. The mean interatomic distances La(1)–O, La(2)–O, and Zr–O were determined to be 2.59 Å, 2.54 Å, and 2.11 Å, respectively. These values were in good agreement with 2.58 Å for La^{3+}–O^{2-} (coordination number (CN): 8) and 2.12 Å for Zr^{4+}–O^{2-} (CN: 6) calculated from Shannon's ionic radii [20].

Li atoms occupied three types of crystallographic site, as shown in Fig. 2. Li(1) atoms occupied tetrahedral 8*a* sites; here the other tetrahedral 16*e* site, which is the equivalent position to the tetrahedral 8*a* site in the cubic garnets, was vacant. Li(2) and Li(3) atoms occupied octahedral 16*f* and 32*g* sites, respectively. Li atoms fill all three sites for tetragonal $Li_7La_3Zr_2O_{12}$. This is an important distinction compared to the cubic garnet-related Li-ion conductors such as $Li_5La_3Ta_2O_{12}$ [2] and $Li_6BaLa_2Ta_2O_{12}$ [4,5]. The Li–Li distances were 2.529(14) Å for Li(1)–Li(3), and 2.57(2) Å and 2.71(2) Å for Li(2)–Li(3). The Li–O interatomic distances were listed in Table 4. The tetrahedral $Li(1)O_4$ was not significantly distorted, and the Li(1)–O distance was 1.886(4) Å. The octahedral $Li(2)O_6$ and $Li(3)O_6$ were distorted, and had two long Li–O bonds of 2.45(2) Å ($\times 2$) for Li(2)–O and 2.81(2) Å and 2.88(2) Å for Li(3)–O. It may be more appropriate to describe the coordination polyhedron of Li(2) and Li(3) sites as a highly distorted tetrahedron. However, the mean distance in octahedral coordination was 2.27 Å for Li(2)–O and 2.31 Å for Li(3)–O. These values are normal for octahedral Li–O coordination.

The ideal garnets $\{C_3\}[A_2](D_3)O_{12}$ have a chain composed of edge-sharing tetrahedral DO_4 and dodecahedral CO_8. Each $[-DO_4-CO_8-]_n$ chain direction coincides with the *a*, *b*, and *c* axes. In the present tetragonal structure of $\{La_3\}[Zr_2](Li_1\square_2)\,Li_6O_{12}$ (□: vacancy), the tetrahedral sites, corresponding to the tetrahedral *D* site (24*d* site) in the ideal garnets, were completely ordered by both Li(1) atoms (8*a* site) and vacancies (16*e* site). Therefore, the only unbroken chain, $[-Li(1)O_4-La(1)O_8-]_n$, ran along the *c* axis. The chains along the *a* and *b* axes were disrupted by the existence of the vacant tetrahedral 16*e* site. The Li–□ ordering in the tetrahedral sites of tetragonal $Li_7La_3Zr_2O_{12}$ may be the origin of the tetragonal symmetry.

Li atoms in the cubic garnet-related Li-ion conducting oxides are located in similar coordinations, with tetrahedra and octahedra similar to the present tetragonal $Li_7La_3Zr_2O_{12}$ [2–5]. These cubic compounds, for instance $Li_5La_3Ta_2O_{12}$ [2], have lower Li content than tetragonal $Li_7La_3Zr_2O_{12}$, and thus show a complicated Li arrangement with Li dimer formation [4] by the complete Li–□ disordering in the tetrahedral and octahedral sites [2,3,5]. This Li arrangement is the significant characteristic of Li-ion conducting oxides with cubic garnet-related type structure. Here, $Li_7La_3Zr_2O_{12}$ has the two stable phases of cubic and tetragonal symmetries. Cubic $Li_7La_3Zr_2O_{12}$ was recently reported by Murugan et al. [1], with only the lattice constant given. The detailed structure analysis has not yet been reported. Let us discuss the cubic $Li_7La_3Zr_2O_{12}$ from the viewpoint of Li arrangement. It is likely that the $Li_7La_3Zr_2O_{12}$ also shows cubic symmetry to allow Li-□ disordering. One possible explanation for this suggestion may be that the Li content in the tetrahedron and the octahedron is decreased by occupation of the vacant trigonal prismatic site by Li atoms, or by the oxygen-deficiency model [6] of $Li_{7-2x}La_3Zr_2O_{12-x}$.

3.3. X-ray and neutron powder diffraction analysis

Fig. 3 shows the XRD pattern of tetragonal $Li_7La_3Zr_2O_{12}$. The structure analysis was conducted by the Rietveld method using the computer program RIETAN-2000. In the structure analysis using the XRD data, all structure parameters were fixed at the results of the single-crystal X-ray analysis presented in Table 2. The XRD pattern was clearly identified to be from a single phase with the tetragonal $Li_7La_3Zr_2O_{12}$ structure determined in this work. Table 5 summarizes the details of the structure refinements and data collection. The final *R*-values were $R_{wp} = 10.92\%$, $R_p = 8.12\%$, $R_B = 3.44\%$, and $R_F = 1.54\%$, with a fit indicator of $S = R_{wp}/R_e = 1.64$. The lattice constants were refined to be $a = 13.130(2)$ Å and $c = 12.675(2)$ Å. The splitting of the diffraction lines, caused by a slight distortion of the tetragonal symmetry, was observed. For example, the splitting corresponding to 4 0 0 and 0 0 4 was clearly observed in the diffraction data around $2\theta = 27^\circ$ and 28°, respectively. It should be noted that no polycrystalline sample having cubic symmetry was observed in the temperature range studied in this work.

Fig. 4 shows observed, calculated, and difference patterns for the Rietveld refinements from the ND data of tetragonal $Li_7La_3Zr_2O_{12}$. A small amount of Li_2CO_3 impurity was detected in the ND data. Mass fractions of these compounds contained in the powder specimen were 0.02 for Li_2CO_3 and 0.98 for tetragonal $Li_7La_3Zr_2O_{12}$ estimated by later Rietveld analysis. This impurity arose from the additional Li_2CO_3 used in sample preparation, with the large amount of 20 g used to measure the ND data. In the structure analysis using the ND data, we adapted the structure model determined from the single-crystal data as the initial structure model. The diffraction peaks in the ND pattern were well-indexed on the basis of tetragonal symmetry with a space

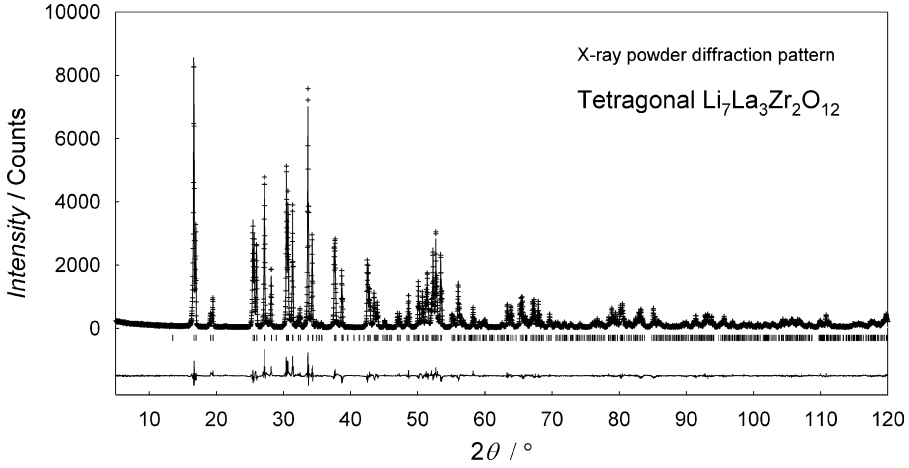

Fig. 3. Observed (+), calculated (solid line), and difference (bottom) patterns for the Rietveld refinement from the X-ray powder diffraction data of tetragonal $Li_7La_3Zr_2O_{12}$. The short vertical lines below the profiles mark the peak positions of all possible Bragg reflections of tetragonal $Li_7La_3Zr_2O_{12}$.

group of $I4_1/acd$, except for peaks from Li_2CO_3 impurity, as shown in Fig. 4. The final R-values reached $R_{wp} = 3.87\%$, $R_p = 2.94\%$, $R_B = 0.76\%$, and $R_F = 0.38\%$, with $S = 1.54$. The lattice constants were refined to be $a = 13.1279(5)$ Å and $c = 12.6715(5)$ Å. Table 6 presents the final structure parameters of tetragonal $Li_7La_3Zr_2O_{12}$ determined from the ND data. Fig. 5 depicts the three-dimensional distribution of nuclear scattering length density for tetragonal $Li_7La_3Zr_2O_{12}$ provided by the MEM analysis. The distribution of all atoms was clearly visible at the appropriate positions in the MEM image. No large unidentified distribution was obtained. Among Li, La, Zr, and O atoms, only the Li atom had a negative nuclear scattering length. The distribution having a negative value was obvious at Li(1), Li(2), and Li(3) sites, and the distribution having a positive value was consistent with the La, Zr, and O sites.

The X-ray and neutron powder diffraction patterns were well-identified with the tetragonal $Li_7La_3Zr_2O_{12}$ structure ($I4_1/acd$, no. 142) determined by the single-crystal analysis. The structure parameters refined using ND data were in good agreement with those determined using the single-crystal data, as presented in Tables 2 and 6. The lattice constants obtained from the X-ray and neutron powder diffraction data were consistent with the results of the single-crystal X-ray analysis, as presented in Tables 1 and 5.

Table 5
Crystallographic data and details of the structure refinement and data collection for X-ray and neutron powder diffraction from tetragonal $Li_7La_3Zr_2O_{12}$ at room temperature.

Chemical formula	$Li_7La_3Zr_2O_{12}$	
Radiation	Cu$K\alpha$	Neutron
Crystal system	Tetragonal	Tetragonal
Space group	$I4_1/acd$ (no. 142)	$I4_1/acd$ (no. 142)
Lattice constant a (Å)	13.130(2)	13.1279(5)
Lattice constant c (Å)	12.675(2)	12.6715(5)
D_x (g cm^{-3})	5.106	5.108
R_{wp} (%)	10.92	3.87
R_e (%)	6.65	2.52
R_p (%)	8.12	2.94
R_B (%)	3.44	0.76
R_F (%)	1.54	0.38
S	1.64	1.54
Wavelength (Å)	1.5418	1.8204(5)
2θ range (deg)	5–120	7–157
2θ step width (deg)	0.02	0.10
Number of relaxed reflections	10	4

The R-factors and S are defined in Ref. [23].

3.4. Ionic conductivity

Fig. 6 illustrates a Nyquist plot of the ac impedance spectra for the sintered sample of tetragonal $Li_7La_3Zr_2O_{12}$. The steep rise of the impedance plot in the low-frequency range is typically

Table 6
Structure parameters determined from neutron powder diffraction data for tetragonal $Li_7La_3Zr_2O_{12}$.

Atom	Site	g	x	y	z	U (Å^2)
La(1)	8b	1	0	1/4	1/8	0.0039(8)
La(2)	16e	1	0.1270(2)	0	1/4	0.0046(6)
Zr	16c	1	0	0	0	0.0048(7)
Li(1)	8a	1	0	1/4	3/8	0.014(3)
Li(2)	16f	1	0.1797(6)	0.4297[(a)]	1/8	0.022(3)
Li(3)	32g	1	0.0806(5)	0.0857(5)	0.8041(5)	0.013(2)
O(1)	32g	1	−0.0338(2)	0.0548(2)	0.1524(2)	0.0046(7)
O(2)	32g	1	0.0541(2)	0.8529(2)	0.5338(2)	0.0067(8)
O(3)	32g	1	0.1496(2)	0.0276(2)	0.4464(2)	0.0050(6)

Linear constraint. (a) $y(\mathrm{Li}(2)) = 0.25 + x(\mathrm{Li}(2))$.

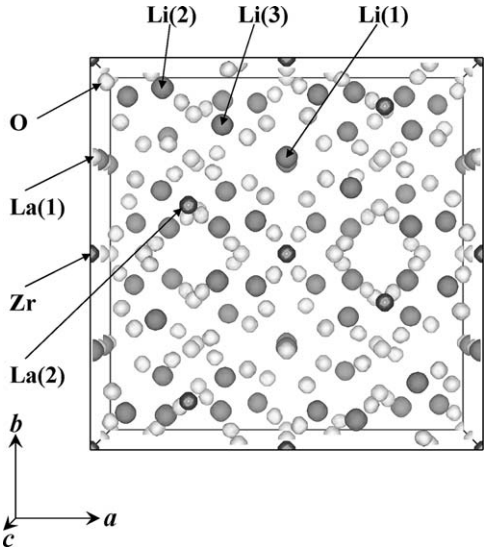

Fig. 5. Three-dimensional distribution of nuclear scattering length density with an iso-surface level of 1.0 fm Å^{-3} for tetragonal $Li_7La_3Zr_2O_{12}$. The distribution is colored gray or white to show a negative or positive nuclear scattering length, respectively. The solid box indicates the unit cell.

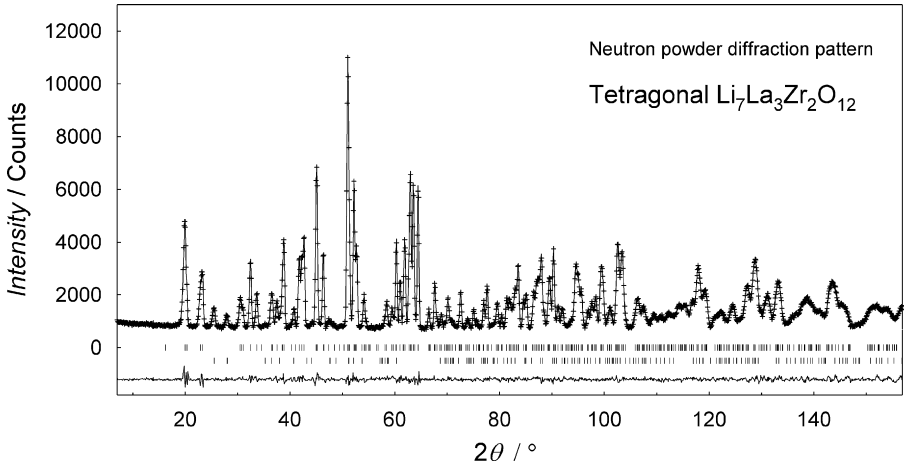

Fig. 4. Observed, calculated, and difference patterns for the Rietveld refinement from the neutron powder diffraction data of tetragonal $Li_7La_3Zr_2O_{12}$. The short vertical lines below the profiles mark the peak positions of all possible Bragg reflections of tetragonal $Li_7La_3Zr_2O_{12}$ (upper) and Li_2CO_3 (lower).

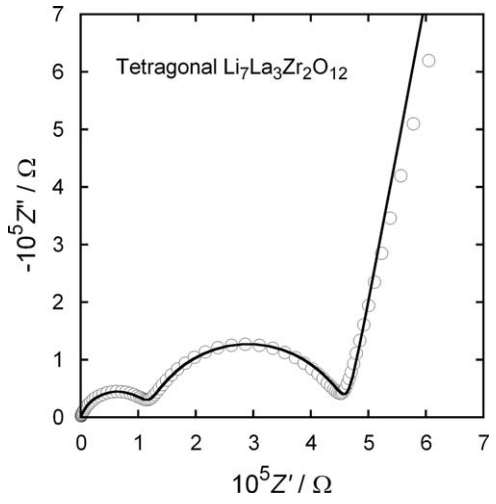

Fig. 6. Nyquist plot of the ac impedance spectra for the sintered sample of tetragonal $Li_7La_3Zr_2O_{12}$ with Li-blocking Au electrodes at 300 K in air. The open circles show experimental results and the solid curve shows the calculated results with an equivalent circuit of $(R_bQ_b)(R_{gb}Q_{gb})(Q_{el})$.

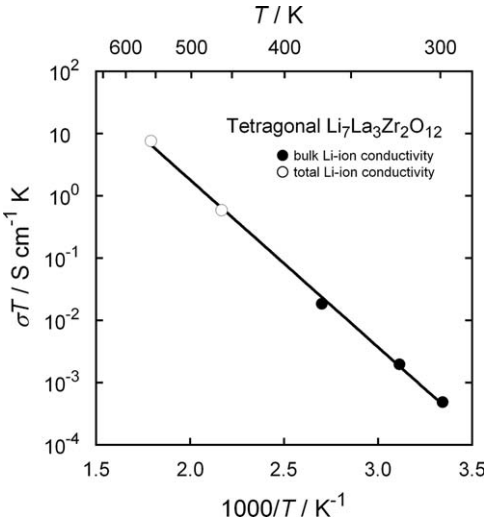

Fig. 7. Temperature dependence of the Li-ion conductivity of tetragonal $Li_7La_3Zr_2O_{12}$. The solid and open circles show bulk Li-ion conductivity and total (sum of the bulk and grain-boundary contributions) Li-ion conductivity, respectively.

expected for the blocking of mobile Li ions at the electrode interface, which is evidence that tetragonal $Li_7La_3Zr_2O_{12}$ is a Li-ion conductor. The impedance plot in the high-frequency range displayed two semicircles. Cubic $Li_7La_3Zr_2O_{12}$ has similar features [1]. The resistance component on the high frequency side was the bulk contribution, and the other was the grain-boundary contribution. Each semicircle was interpreted as an equivalent circuit consisting of a parallel combination of a resistance and a capacitance. The overall behavior of the impedance plot can be fitted by an equivalent circuit of $(R_bQ_b)(R_{gb}Q_{gb})(Q_{el})$, where R is the resistance, Q the constant phase element for the capacitive element, and the subscripts b, gb, and el with each notation represent the bulk, grain-boundary, and electrode, respectively. The conductivities were obtained by analyzing the impedance plots using a computer program ZView3.0. The bulk Li-ion conductivity was $\sigma_b = 1.63 \times 10^{-6}$ S cm^{-1}, and the grain-boundary Li-ion conductivity was $\sigma_{gb} = 5.59 \times 10^{-7}$ S cm^{-1} at 300 K ($\sigma_b = 5.68 \times 10^{-6}$ S cm^{-1} and $\sigma_{gb} = 3.57 \times 10^{-6}$ S cm^{-1} at 320 K). Thick-pellet cubic $Li_7La_3Zr_2O_{12}$ was reported to be a fast Li-ion conductor with a high bulk conductivity of $\sigma_b = 4.67 \times 10^{-4}$ S cm^{-1} at 298 K and $\sigma_b = 1.19 \times 10^{-3}$ S cm^{-1} at 323 K [1]. About two orders of magnitude lower bulk Li-ion conductivity was observed for tetragonal $Li_7La_3Zr_2O_{12}$ compared to cubic $Li_7La_3Zr_2O_{12}$ at 300 and 320 K.

Fig. 7 shows the Li-ion conductivity as a function of $1/T$ for a sintered sample of $Li_7La_3Zr_2O_{12}$. The conductivity could not be separated into bulk and grain-boundary contributions above 370 K, therefore the total (sum of the bulk and grain-boundary contributions) Li-ion conductivity was plotted above 370 K in Fig. 7. The temperature dependence of the conductivity can be expressed by the Arrhenius equation,

$$\sigma = \frac{A}{T}\exp\left(\frac{-E_a}{k_BT}\right), \quad (2)$$

where A is the pre-exponential factor, T the absolute temperature, E_a the activation energy, and K_B the Boltzmann constant. The activation energy was estimated to be $E_a = 0.54$ eV from the slope of the $\log \sigma T$ versus $1/T$ plot in the temperature range of 300–560 K.

Tetragonal $Li_7La_3Zr_2O_{12}$ showed a lower Li-ion conductivity than the garnet-related Li-ion conductor having cubic symmetry, for instance, $\sigma_b = 5.11 \times 10^{-4}$ S cm^{-1} at 298 K ($E_a = 0.30$ eV) for cubic $Li_7La_3Zr_2O_{12}$ [1] and $\sigma_b = 4.0 \times 10^{-5}$ S cm^{-1} at 295 K ($E_a = 0.47$ eV) for $Li_5La_3Bi_2O_{12}$ [7]. This result may be discussed in terms of the Li arrangement based on the crystal structure analysis. According to a previous report [8], the Li-ion conduction pathway of the garnet-related Li-ion conductors is composed of the face-sharing tetrahedral and octahedral Li sites. For the present tetragonal $Li_7La_3Zr_2O_{12}$, these tetrahedral and octahedral sites were completely ordered by Li atoms and vacancies. On the other hand, the cubic garnet-related compounds showed a complicated Li–□ disordering on these tetrahedral and octahedral sites. Moreover, many vacant Li sites were located in the Li-ion conduction pathway in comparison to tetragonal $Li_7La_3Zr_2O_{12}$, because of an increase in an equivalent position to the Li site by the high symmetry of Ia–$3d$ for cubic garnet-related compounds [2–5]. It should be concluded that suppressed hopping between Li sites by the complete Li–□ ordering, and the decrease in equivalent Li positions compared to the cubic garnet-related compounds may result in the low Li-ion conduction of the present tetragonal $Li_7La_3Zr_2O_{12}$.

For $(Li_3)\{Ln_3\}[Te_2]O_{12}$ (Ln = Y, Pr, Nd, Sm–Lu) with a relatively lower Li content, the Li atoms in these compounds were fully ordered on the tetrahedral D site in the ideal garnet structure $\{C_3\}[A_2](D_3)O_{12}$ with cubic symmetry (Ia–$3d$). $Li_3Nd_3Te_2O_{12}$ demonstrated a much lower Li-ion conductivity, around 10^{-5} S cm^{-1} at 873 K [21]. The Li concentration of $Li_3Nd_3Te_2O_{12}$ could be increased by substitution of Te^{6+} ions by Sb^{5+} ions [22]. $Li_{3+x}Nd_3Te_{2-x}Sb_xO_{12}$ ($0<x<2$) had a garnet-related structure with Li–□ disordering at increased Li concentrations. The Li-ion conductivity of $Li_{3+x}Nd_3Te_{2-x}Sb_xO_{12}$ increased by several orders of magnitude compared to $Li_3Nd_3Te_2O_{12}$ with the fully ordered arrangement of Li atoms. There are strong parallels between these compounds [21,22] and the ordered (tetragonal $Li_7La_3Zr_2O_{12}$) and disordered (cubic garnet-related Li-ion conductors) phases.

4. Conclusion

Garnet-related type $Li_7La_3Zr_2O_{12}$ with tetragonal symmetry was successfully synthesized by a solid-state reaction for the first time. The chemical composition of the fine-powder specimen was determined to be $Li_7La_3Zr_2O_{12}$ by ICP-OES analysis. Single crystals of this compound were also successfully grown by a flux method. Single-crystal X-ray diffraction analysis verified that tetragonal $Li_7La_3Zr_2O_{12}$ had a garnet-relayed type structure with a space group

$I4_1/acd$ (no. 142). The lattice constants were $a = 13.134(4)$ Å and $c = 12.663(8)$ Å. The garnet-type framework structure was composed of dodecahedral $La(1)O_8$, $La(2)O_8$, and octahedral ZrO_6. Li atoms occupied three types of crystallographic sites in the interstices of this framework structure, where Li(1), Li(2), and Li(3) atoms were located in the tetrahedral 8*a* site and the distorted octahedral 16*f* and 32*g* sites, respectively. Li atoms filled all three sites. This is an important distinction compared to the cubic garnet-related Li-ion conductors. The structure was also investigated by the Rietveld method using X-ray and neutron powder diffraction data. These diffraction patterns were identified as the tetragonal $Li_7La_3Zr_2O_{12}$ structure determined from the single-crystal data. The bulk Li-ion conductivity of tetragonal $Li_7La_3Zr_2O_{12}$ was $\sigma_b = 1.63 \times 10^{-6}\,S\,cm^{-1}$, and the grain-boundary Li-ion conductivity was $\sigma_{gb} = 5.59 \times 10^{-7}\,S\,cm^{-1}$ at 300 K. The activation energy was estimated to be $E_a = 0.54$ eV in the temperature range of 300–560 K.

Acknowledgment

This research was supported by Research Fellowships from the Japan Society for the Promotion of Science for Young Scientists (18–1415).

References

[1] R. Murugan, V. Thangadurai, W. Weppner, Angew. Chem. Int. Ed. 46 (2007) 7778.
[2] E.J. Cussen, Chem. Commun. (2006) 412.
[3] J. Percival, P.R. Slater, Solid State Commun. 142 (2007) 355.
[4] M.P. O'Callaghan, E.J. Cussen, Chem. Commun. (2007) 2048.
[5] J. Awaka, N. Kijima, Y. Takahashi, H. Hayakawa, J. Akimoto, Solid State Ionics 180 (2009) 602.
[6] R. Murugan, V. Thangadurai, W. Weppner, Appl. Phys. A91 (2008) 615.
[7] R. Murugan, W. Weppner, P. Schmid-Beurmann, V. Thangadurai, Mater. Sci. Eng. B143 (2007) 14.
[8] V. Thangadurai, S. Adams, W. Weppner, Chem. Mater. 16 (2004) 2998.
[9] S.R. Hall, D.J. du Boulay, R. Olthof-Hazekamp, Eds. Xtal3.7 System, University of Western Australia, 2000.
[10] K. Ohoyama, T. Kanouchi, K. Nemoto, M. Ohashi, T. Kajitani, Y. Yamaguchi, Jpn. J. Appl. Phys. 37 (1998) 3319.
[11] F. Izumi, T. Ikeda, Mater. Sci. Forum 321–324 (2000) 198.
[12] F. Izumi, R.A. Dilanian, Recent Research Developments in Physics, vol. 3, Part II, Transworld Research Network, Trivandrum, 2002, p. 699.
[13] K. Momma, F. Izumi, Comm. Crystallogr. Comput. IUCr Newslett. 7 (2006) 106.
[14] J.V. Smith, B. Mason, Science 168 (1970) 832.
[15] A. Nakatsuka, A. Yoshiasa, T. Yamanaka, O. Ohtaka, T. Katsura, E. Ito, Am. Miner. 84 (1999) 1135.
[16] K.-H. Hellwege (Ed.), Magnetic and Other Properties of Oxides and Related Compounds, Part b: Landolt-Börnstein, New Series, Group III: Crystal and Solid State Physics, vol. 4, Springer, Berlin, Heidelberg, New York, 1970, p. 1. (and references therein).
[17] J. Awaka, R. Katagi, H. Sasaki, R. Endoh, N. Matsumoto, S. Ebisu, S. Nagata, J. Phys. Chem. Solids 62 (2001) 743.
[18] J. Awaka, R. Endoh, S. Nagata, J. Phys. Chem. Solids 64 (2003) 2403.
[19] J. Awaka, M. Ito, T. Suzuki, S. Nagata, J. Phys. Chem. Solids 66 (2005) 851.
[20] R.D. Shannon, Acta Crystallogr. A 32 (1976) 751.
[21] M.P. O'Callaghan, D.R. Lynham, E.J. Cussen, G.Z. Chen, Chem. Mater. 18 (2006) 4681.
[22] M.P. O'Callaghan, A.S. Powell, J.J. Titman, G.Z. Chen, E.J. Cussen, Chem. Mater. 20 (2008) 2360.
[23] R.A. Young (Ed.), The Rietveld Method, Oxford University Press, Oxford, 1995 (Chapter 1).